

Article

Coal as an Effective Catalyst for Selective Oxidative Dehydrogenation of Propane to Propene

Qiuwen Liu^{1,2,*}, Yuhua Zhang¹, Yawei Wu¹, Mingxia Song³ and Caijin Huang^{1,*}

¹ State Key Laboratory of Photocatalysis on Energy and Environment, College of Chemistry, Fuzhou University, Fuzhou 350116, China

² Ganjiang Innovation Academy, Chinese Academy of Sciences, Ganzhou 341000, China

³ Collaborative Innovation Center of Atmospheric Environment and Equipment Technology (CICAET), School of Environmental Science and Engineering, Nanjing University of Information Science and Technology, Nanjing 210044, China

* Correspondence: qiuwenl@gia.cas.cn (Q.L.); cjhuang@fzu.edu.cn (C.H.)

Abstract: Coal is a readily available and inexpensive material. However, its direct use as a catalyst is still rare, but attractive for practical application. In this paper, coal was directly used as a catalyst for the selective oxidative dehydrogenation of propane to propene. It exhibited a high selectivity over 90% with a yield of 8.4% at a high space velocity (12,000 mL·(h·g-cat)⁻¹). The productivity up to 2.84 gC₃H₆ g_{cat}⁻¹ h⁻¹ was obtained with propene selectivity above 80% (20,000 mL·(h·g-cat)⁻¹). The kinetic showed first-order dependence with respect to propane or oxygen partial pressures. Meanwhile, electron paramagnetic resonance (EPR) and X-ray photoelectron spectrum (XPS) demonstrated that the carbonyl groups act as active sites for oxidative dehydrogenation of propane to propene. This work expands the use of earth-abundant and low-price coal in catalysis with expectable scale application.

Keywords: coal; catalysis; kinetics; oxidative dehydrogenation; propane; propene



Citation: Liu, Q.; Zhang, Y.; Wu, Y.; Song, M.; Huang, C. Coal as an Effective Catalyst for Selective Oxidative Dehydrogenation of Propane to Propene. *Catalysts* **2023**, *13*, 628. <https://doi.org/10.3390/catal13030628>

Academic Editors: Bo Weng, Xiaoyang Pan and Bin Han

Received: 6 March 2023

Revised: 19 March 2023

Accepted: 20 March 2023

Published: 21 March 2023



Copyright: © 2023 by the authors. Licensee MDPI, Basel, Switzerland. This article is an open access article distributed under the terms and conditions of the Creative Commons Attribution (CC BY) license (<https://creativecommons.org/licenses/by/4.0/>).

1. Introduction

Propene, one of the main raw materials in industrial synthesis, can be used as a building block to produce polypropylene, acrylonitrile, isopropanol, acetone, epoxypropane, etc. Its annual consumption has reached ca. 8×10^7 t, and continues to grow as a result of increasing global population [1]. The production of propene mainly depends on steam cracking, fluid catalytic cracking, and catalytic dehydrogenation methods [2,3]. Among them, the methods of steam cracking and fluid catalytic cracking in which oil acts as the basic source are limited by the increasing depletion of oil resources and growing environmental awareness. Meanwhile, the catalytic direct dehydrogenation method suffers coking and limited propene conversion that results from dehydrogenation's thermodynamic constraint [3–6]. For catering to the market, therefore, research on catalytic oxidative dehydrogenation of propane to propene has boomed in the past decades owing to the advantages of anti-coking, energy conservation, and no thermodynamic constraint [2,7,8].

In general, catalysts play an important role in the selectivity and conversion of a catalytic selective oxidative dehydrogenation reaction [2,9,10]. The most commonly used catalysts of oxidative dehydrogenation usually consist of metal-based materials, such as vanadium-based and molybdenum-based materials [11–14]. For example, V-Mg-O was used for the catalytic oxidative dehydrogenation of propane and had a 10% conversion and a propene selectivity of 65% [15]. MoO₃/γ-Al₂O₃ catalysts with different Mo loadings exhibited a propene selectivity less than 60% with a yield less than 10% [16]. However, there are some defects of scale application for metal-based catalysts, such as the low selectivity and pollution of heavy metal [17,18]. Therefore, it is expected that new catalysts of energy conservation, environment protection, and high activity will be explored. Carbon-based

catalysts, as non-metal catalysts, have advantages of widespread source and environmental protection, which have attracted more attention in catalysis over recent decades. In 2001, Schlögl's group first found that carbon nanofilaments have catalytic activity in the oxidative dehydrogenation of ethylbenzene to styrene [19]. They also reported that onion-like carbon materials can be used to catalyze the oxidative dehydrogenation synthesis of ethylbenzene [20]. To date, many carbon nanomaterials (e.g., carbon nanotubes, fullerene-like carbon materials, and nanodiamond) have been used in selective oxidative dehydrogenation reactions [21–23]. Moreover, some bulk carbon materials also showed good performance in selective oxidative dehydrogenation [24–26]. For instance, highly ordered mesoporous carbon gave a 52.4% yield (76% selectivity) for the selective oxidative dehydrogenation of ethylbenzene to styrene [24]. Activated carbon was also used for the conversion of isobutane to isobutene, achieving a stable selectivity of 65% at a conversion of 13% [25]. Castanea mollissima shell-derived porous carbons displayed a more than 90% selectivity (ca. 10% conversion) for the propane dehydrogenation to propylene [26]. Nevertheless, these carbon materials share some common shortcomings of complex preparation procedures and relatively high cost, which restrict their applications. Very recently, Hermans reported that boron nitride can be used as catalyst for selective oxidative dehydrogenation with a propene selectivity of 79% (14% conversion) [27]. However, synthesis of boron nitride at high temperature is energy intensive. Hence, the earth-abundant and low-price catalyst is always expected to meet practical application.

Coal is a readily available and inexpensive material, whose proven reserve is up to ca. 800 billion tonnes in 2005 [28]; however, there are few reports on the use of coal as catalyst [29,30]. Encouragingly, Zhang et al. used coal char catalyst for CO₂ reforming of CH₄ to syngas [29]. However, the coal char catalyst was prepared by pyrolysis of coal at 1150 °C. Furthermore, the kinetic of coal in selective oxidative dehydrogenation reaction has not been discussed enough. In this report, we directly used raw coals as catalysts for the selective oxidative hydrogenation of propane to propene, and acquired an excellent selectivity (as high as 90%) and a good propene yield (8.4%) at a high gas hourly space velocity (12,000 mL·(h·g-cat)⁻¹). The productivity up to 2.84 gC₃H₆ g_{cat}⁻¹ h⁻¹ was obtained with propene selectivity above 80% (20,000 mL·(h·g-cat)⁻¹), which is better than that of most metal-based catalysts. Moreover, the kinetic and activation energy were studied by changing oxygen or propane partial pressures and reaction temperatures. By electron paramagnetic resonance (EPR), X-ray photoelectron spectroscopy (XPS), and attenuated total internal reflectance Fourier-transform infrared spectroscopy (ATR-FTIR) characterization the C=O group was further confirmed as active site. Moreover, we also compared catalytic activity of coal with that of other carbon-based materials. Finally, a possible mechanism is proposed based on our experiment results. This research found coal to be a good catalyst for oxidative dehydrogenation, expanding the application of coal in catalysis.

2. Results and Discussion

2.1. Catalytic Performances of the Catalysts

Three raw coal samples were chosen for use in this work and marked as L-coal, H-coal, and Y-coal, respectively, according to their suppliers. The photos and similar BET surface areas of the three coal samples are displayed in Figures S1 and S2, respectively. Figure 1 shows the catalytic performance of the oxidative dehydrogenation of propane to propene over various raw coals. All coal powders showed similar activity with a 5–10% conversion for propane, and the main product was propene with about 90% selectivity. It indicates that the raw coals have activity and selectivity comparable to nanocarbon catalysts [31,32]. The conversion was not improved obviously, and even decreased with increasing temperature, which differs from common metal oxides catalysts (e.g., V₂O₅ and MoO_x) with temperature-sensitive conversions [33,34]. The similar downtrend of the conversion can also be observed in carbon-based materials (e.g., active carbon and carbonized glucose) (Figure S3). The anomaly in the conversion trend could be caused by

limited oxygen condition; that is, oxygen is consumed by not only propane oxidation, but also thermal decomposition of coal at high temperatures [35]. In order to gain more insight into this phenomenon, L-coal was chosen as the research object due to the better activity at high temperatures. Carbon balance and thermo gravimetric (TG) analysis have been studied together (Figure S4). Compared to input propane, the carbon balance holds stable with increasing temperature when CO_x species is excluded in the final products, indicating that the CO_x products from propane can be neglected (Figure S4a). In contrast, the carbon balance grows when CO_x species is involved along with a slight decrease in coal mass (Figure S4b), demonstrating that these CO_x species mainly come from coal combustion. In addition, the selectivity of CO_x species was calculated to be 4–6.4% (450–550 °C) when L-coal acted as catalyst. Although the combustion of coal consumes a small fraction of oxygen, coals still have superior propene selectivity.

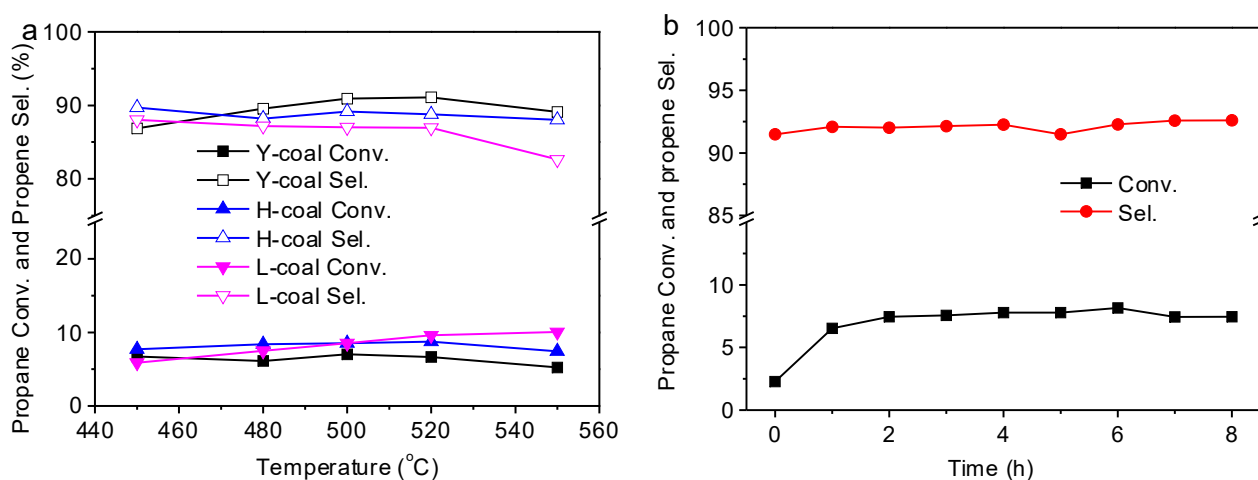


Figure 1. (a) Catalytic performances of three coal samples. (b) The long-time performance of L-coal at 480 °C. Reaction conditions: 15 kPa O_2 , 30 kPa C_3H_8 , N_2 balance, mass space velocity $4000 \text{ mL}\cdot(\text{h}\cdot\text{g}\cdot\text{cat})^{-1}$, 0.3 g catalyst.

Moreover, the higher mass space velocities in the reaction were carried out to obtain the optimized productivity. As shown in Table 1, the better productivity of $2.84 \text{ gC}_3\text{H}_6 \text{ g}_{\text{cat}}^{-1} \text{ h}^{-1}$ was acquired at a higher mass space velocity ($20,000 \text{ mL}\cdot(\text{h}\cdot\text{g}\cdot\text{cat})^{-1}$), which is better than that of most metal-based catalysts according to Cavani's review [2]. Noted that, the C_3H_6 yield grows with increasing space velocity at the range of $4000\text{--}20,000 \text{ mL}\cdot(\text{h}\cdot\text{g}\cdot\text{cat})^{-1}$. However, the decreased yield at $40,000 \text{ mL}\cdot(\text{h}\cdot\text{g}\cdot\text{cat})^{-1}$ could be due to the diffusion control. The abnormally increased conversion at the range of $4000\text{--}20,000 \text{ mL}\cdot(\text{h}\cdot\text{g}\cdot\text{cat})^{-1}$ should be due to the more amount oxygen molecular input, leading to self-combustion of coal and higher fixed bed temperature. For comparison, some carbon-based catalysts and hexagonal boron nitride (BN) were also chosen to investigate their activity of oxidative dehydrogenation of propane (Table 1). Coal has a good catalytic performance (conversion, selectivity, and yield), comparable to other carbon-based materials (active carbon and black carbon) under the same conditions. Most importantly, coal is very cheap, abundant, and can be directly used without any pre-treatment.

Furthermore, L-coal was used to study the long-time performance. Figure 1b manifests a good activity of L-coal at 480 °C for 8 h. The conversion of propane was 2.3% at initial time and then increased rapidly to ca. 7% with a stable propene selectivity of ca. 91%, which could be due to the activation process of coal powder at the initial period.

Table 1. The catalytic activities of various carbon-based catalysts and hexagonal boron nitride (BN).

Sample	Propane Conversion (%)	Propene Selectivity (%)	Propene Yield (%)	Productivity ($\text{gC}_3\text{H}_6 \text{ g}_{\text{cat}}^{-1} \text{ h}^{-1}$)
L-coal ^a	3.1	94.3	2.9	2.17
L-coal ^b	9.4	81.0	7.6	2.84
L-coal ^c	9.3	90.0	8.4	1.89
L-coal ^d	8.6	87.6	7.5	0.56
BN ^d	10.6	76.3	8.1	0.61
Active carbon ^d	13.2	84.7	11.2	0.84
Black carbon ^d	13.3	90.0	12.0	0.90
Graphite ^d	0.7	97.0	0.7	0.053
No catalyst ^d	0.1	8.2	0.1	0.0075

Reaction conditions: 15 kPa O₂, 30 kPa C₃H₈, N₂ balance, 500 °C, 300 mg catalyst, 20–40 mesh. (a–d) Mass space velocity is 40,000, 20,000, 12,000, and 4000 mL·(h·g-cat)^{−1}, respectively.

2.2. Catalytic Kinetics

For the insight of catalytic behavior under various environments, L-coal was used for further experiments. For convenient control of oxygen concentration (P_{O_2}), a higher mass space velocity 12,000 mL·(h·g-cat)^{−1} was chosen. Figure 2 shows the rate of propane consumption as a function of P_{O_2} at a given propane partial pressure ($P_{\text{C}_3\text{H}_8}$). At the lower temperature (450 °C) or $P_{\text{O}_2} (\leq 0.15 \text{ atm})$, the rate of propane consumption increases linearly with increasing of P_{O_2} , indicating the first-order rate dependence with respect to P_{O_2} . However, at the higher temperatures ($\geq 480 \text{ °C}$) and $P_{\text{O}_2} (\geq 0.15 \text{ atm})$, the rate of propane consumption holds stable which follows the zero-order dependence with respect to P_{O_2} , suggesting that the reaction rate is limited by the diffusion-controlled process instead of the surface kinetic-controlled process. This accounts for the higher productivities at higher mass space velocities. The kinetic behavior of oxygen over coal clearly differs from that of traditional supported vanadia catalysts that typically lead to zero-order rate dependence with respect to P_{O_2} [36] and nanocarbon catalysts that make no difference at oxygen pressures higher than 0.01 atm [37]. Meanwhile, after excluding the effect of diffusion control, the apparent activation energy was determined to be 231 kJ/mol under 0.075 atm P_{O_2} (Figure 2b). This value is higher than that of CNT (117 kJ/mol) [38] and of VO_x/ZrO₂, MoO_x/ZrO₂, WO_x/ZrO₂ (48–61 kJ/mol) [39], but it is still lower than boron nitride (BN) catalyst (ca. 253 kJ/mol) [27].

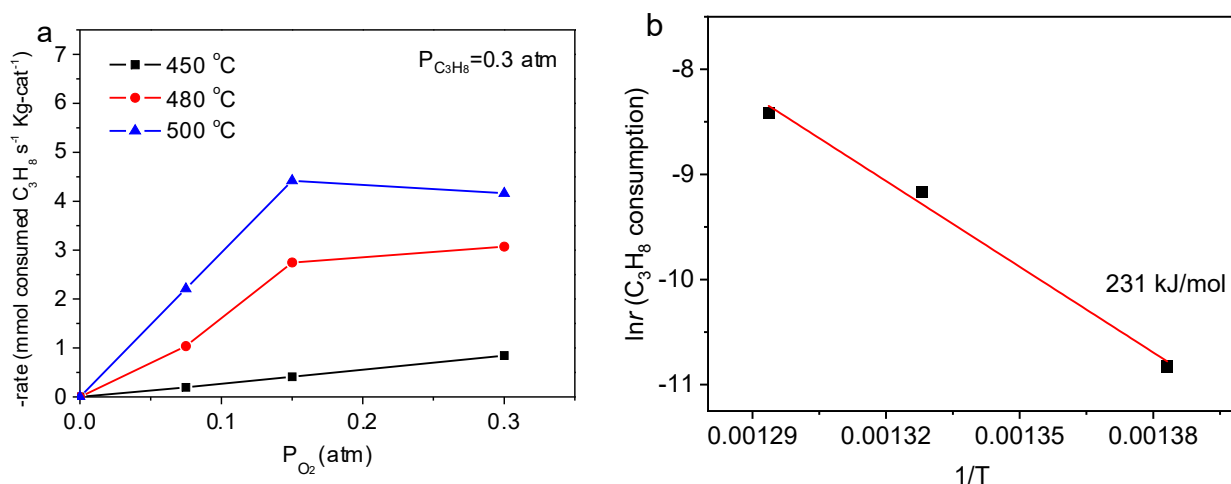


Figure 2. (a) Rates of propane consumption as a function of P_{O_2} ($P_{\text{C}_3\text{H}_8}$ constant at 0.3 atm). (b) Arrhenius plot at 7.5 kPa P_{O_2} . Reaction conditions: various partial pressures of O₂ are 7.5, 15, or 30 kPa, 30 kPa C₃H₈, N₂ balance, mass space velocity 12,000 mL·(h·g-cat)^{−1}, 0.3 g L-coal, 20–40 mesh.

Figure 3 displays the rate of propane consumption as a function of $P_{C_3H_8}$ at a given P_{O_2} . The rate of propane consumption increased linearly with its increasing partial pressure (0–0.2 atm), which is in agreement with the previous carbon-based report [37]. This indicates the first-order rate dependence with respect to propane.

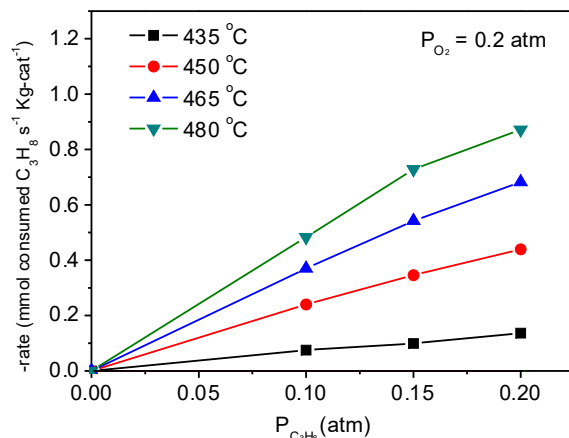


Figure 3. Rates of propane consumption as a function of $P_{C_3H_8}$ (P_{O_2} constant at 0.2 atm) with linear fitting. Reaction conditions: N_2 balance, mass space velocity $4000 \text{ mL} \cdot (\text{h} \cdot \text{g-cat})^{-1}$, 0.3 g L-coal, 20–40 mesh.

To investigate the role of the carbon-based part in coal, the control experiment was carried out by using L-coal, overused L-coal, and L-coal residue. L-coal powder after reaction under 30 kPa P_{O_2} was named as overused L-coal powder. L-coal powder after burning out at 700 °C for 2 h under air atmosphere was marked as coal residue. Figure 4 shows that overused L-coal powder is partially burned and contains a small amount of carbon (Figure S5). L-coal residue does not contain carbon-based part and represents other components in coal. In Figure S5d, the L-coal, overused L-coal, and L-coal residue show conversions of ca. 8.0%, 1.5%, and 1.3%, respectively, meaning that the coal residue has a small effect on catalytic dehydrogenation, but the carbon-based part plays a pivotal role in catalysis.

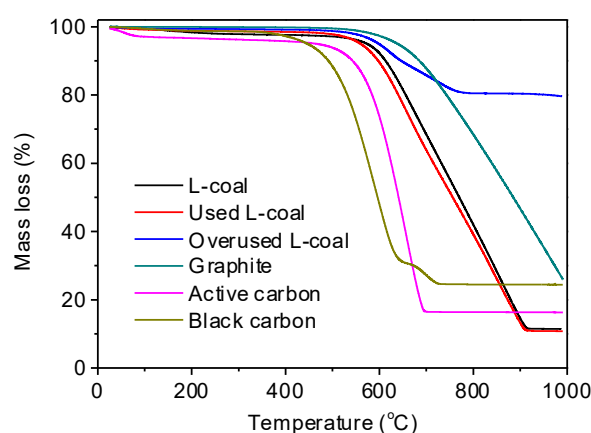


Figure 4. TG data of coal and various carbon materials in air (20 mL/min). L-coal powder after reaction under 30 kPa P_{O_2} was named as overused L-coal powder. The used L-coal is the raw L-coal after reaction under 7.5 kPa O_2 at below 500 °C.

2.3. Characterizations of the Catalysts

Thermo gravimetry (TG) analysis was often used to characterize the stability of the materials under ambient atmosphere. As shown in Figure 4, L-coal powder, used L-coal powder, and overused L-coal powder began to lose their mass at ca. 500 °C. The mass

loss mainly comes from the high-temperature decomposition of the carbon part of coal. Active carbon and black carbon began their mass loss at lower temperatures (ca. 450 and ca. 400 °C, respectively), but graphite started at ca. 600 °C. Additionally, both L-coal powder and used L-coal powder manifested the biggest mass loss ca. 90%; that is to say, the carbon content in L-coal powder barely changed. Moreover, L-coal powder and used L-coal powder have high similarity in XRD patterns (Figure S6) and no obvious change in morphology by SEM observation (Figure S7), revealing that coal is relatively stable during the reaction at low oxygen partial pressures (7.5 kPa) and low temperatures (<500 °C).

Electron paramagnetic resonance (EPR) spectrum is often used to study free radicals in coal [20]. Figure 5 depicts the EPR spectra of L-coal powder and used L-coal powder. The g value of L-coal powder at 2.0041 belongs to π -type oxygen in free radicals such as quinones (1–3 rings) and ethers [40]. The g values of used L-coal powder decreased to 2.0032, which could be caused by the formation of considerable σ -type oxygen in the free radicals of hydroxyl produced through hydrogen extraction [40,41]. The signal intensity of the free radicals of used L-coal powder increased by an order of magnitude than L-coal powder. This is possibly due to much more formation of oxygen-containing functional groups that mainly include carbonyl (C=O) and hydroxyl (C-OH) groups in oxidation reaction [41–43]. These oxygen-containing functional groups can also be detected by X-ray photoelectron spectroscopy (XPS) (Figure 6). According to Su's report [37], carbonyl group is the main active site in oxidative dehydrogenation reaction. Therefore, it can be concluded that coal is activated by oxygen and thus produces oxygen-containing active sites (C=O) to catalyze the dehydrogenation of propane to propene.

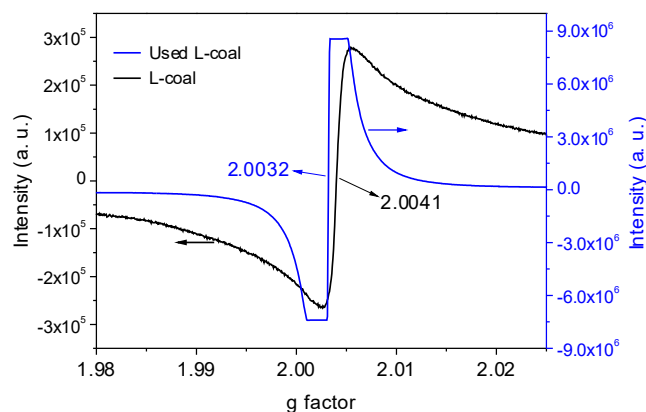


Figure 5. EPR spectra of L-coal powder and used L-coal powder.

X-ray photoelectron spectroscopy (XPS) was used to further investigate the chemical component state on coal surface and provided some information on reaction mechanism. Figure 6a,b show that oxygen, carbon, and some impurities elements existed in both L-coal powder and used L-coal powder samples. The used L-coal is the raw L-coal after reaction under 7.5 kPa O₂ at temperature below 500 °C. By comparing XPS spectra of the two samples, the content of surface carbon of used L-coal powder (65.4 atomic%) decreased with increasing oxygen element, indicating oxygen has been adsorbed or bonded to carbon on the coal surface. Moreover, the C 1s core-level spectra (Figure 6c) were composed of three parts of C–C (284.4 eV), C–O (295.8 eV), and C=O (288.5 eV) bonds. The used L-coal powder showed obviously stronger C–O and C=O bond signals, which can also be observed by IR analysis (Figure S8). This indicates that there is a high content of C=O groups in used L-coal powder [22]. Meanwhile, used L-coal powder has a stronger O 1s signal made up of O=C, O–C, and O–H at 531.4, 532.4, and 533.7 eV, respectively (Figure 6d). In view of the pivotal role of C–OH and C=O in oxidative dehydrogenation reaction [26,37], the higher content of oxygen-containing moieties could be attributed to the activation process at the initial stage of reaction, which can be verified by the presence of activation process appearing in long-time performance (Figure 1b).

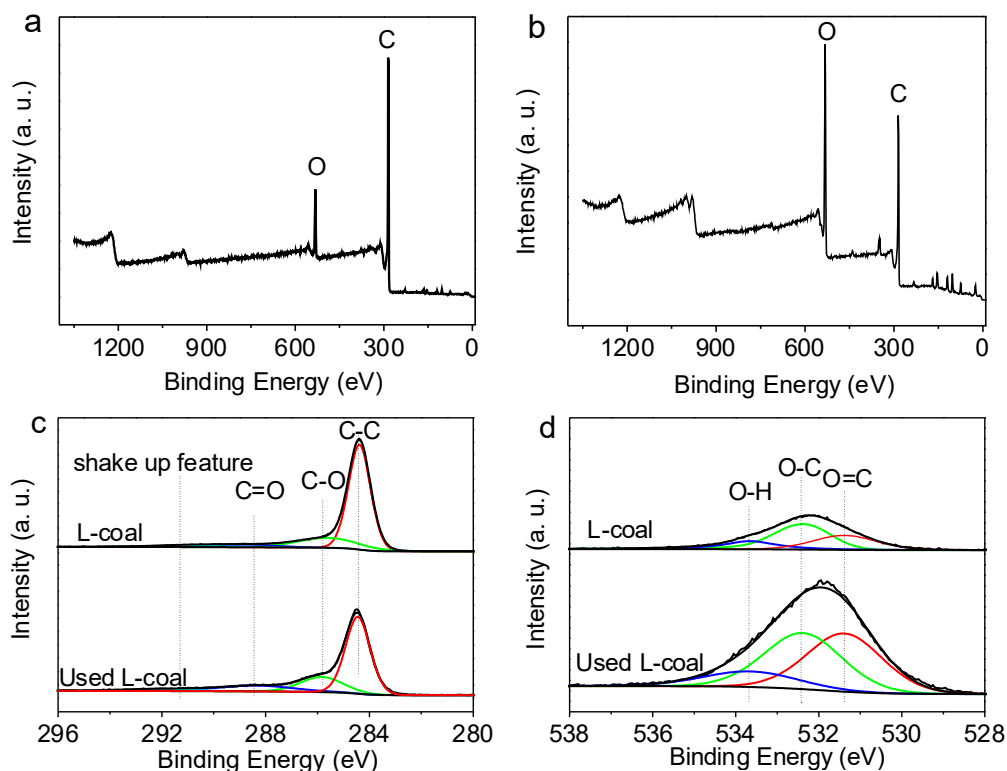


Figure 6. XPS spectra of (a) L-coal powder and (b) used L-coal powder, (c) C 1s core-level spectrum and (d) O 1s core-level spectrum of L-coal powder and used L-coal powder.

The effect of oxygen on the catalytic activity of L-coal was studied to further verify the active site (C=O) by switching on or off oxygen feeding during the reaction (Figure 7). When switching off oxygen feeding, the catalytic activity was relatively higher at initial time under nitrogen atmosphere, which could be due to the existence of natural carbonyl group in L-coal [44]. The presence of natural carbonyl group in raw coal can be confirmed by XPS analysis (Figure 6). However, the conversion decreases as the reaction progresses, which can be explained by the consumption of carbonyl groups, namely, the decreased active sites [24,44]. Moreover, when oxygen was re-introduced into the reaction system, the conversion gradually recovered due to the newly formed carbonyl groups on the coal surface.

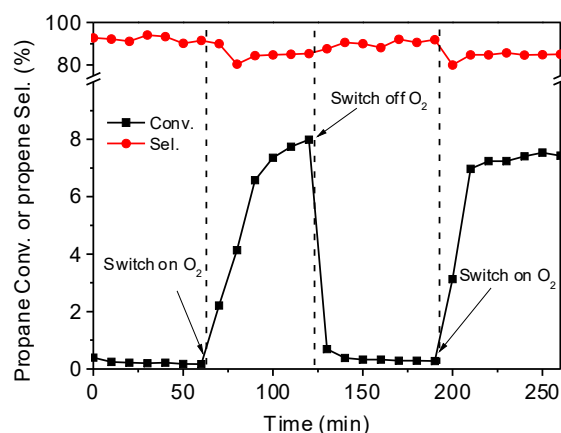


Figure 7. The effect of oxygen on catalytic activity over L-coal by switching on or off oxygen feeding. Reaction conditions: 30 kPa C_3H_8 , with or without 15 kPa O_2 , N_2 balance, mass space velocity $4000 \text{ mL} \cdot (\text{h} \cdot \text{g} \cdot \text{cat})^{-1}$, $480 \text{ }^\circ\text{C}$. 0.3 g catalyst, 20–40 mesh.

2.4. The Possible Mechanism

Generally, two main mechanisms (free radical reaction mechanism [45] and redox mechanism [36]) have been developed to explain the catalytic phenomenon on the oxidative dehydrogenation of alkane. The free radical mechanism is usually used for high temperature environment ($>450\text{ }^{\circ}\text{C}$), while redox mechanism is applicable to metal oxides catalysts. Su et al. reported that due to the unique chemical structure of nanocarbon materials, the reaction mechanism is different from typical Mars–van Krevelen (redox mechanism) or Langmuir–Hinshelwood models [37]. They proposed that both the free radical mechanism and the redox mechanism are involved for carbon-based materials in their work.

In our work, in respect of the catalyst, the carbon-based part of coal was identified as the active component. The C=O group has been proven as the active site, which is consistent with the previous reports [21,37,44]. There is a circulation between C=O and C–OH groups. Therefore, the redox process plays an important role in oxidative dehydrogenation in our system. On the other hand, as for propane, there is a process of H atom abstraction from propane and thus formation of isopropyl, which has been confirmed by some theory calculations [37,46,47]. Then, another H atom linked to the adjacent carbon is abstracted, resulting in the production of propene. Hence, the free radical mechanism is also involved.

Based on the above discussions and some previous reports [24,26,37,48], a mechanism involving both redox mechanism and free radical mechanism is proposed (Figure 8). With rising temperature, oxygen is introduced into the coal surface accompanying with the formation of carbonyl (C=O) group. Due to the nature of the Lewis base, the newly generated and original C=O group acts as the electron donor and becomes the active sites for activating the C–H bond of the propane [49,50]. The C=O group extracts a hydrogen atom from propane, which forms hydroxyl (C–OH) and isopropyl groups as intermediate products. Then, the isopropyl group loses its second hydrogen atom captured by another C=O and is converted into propene. Subsequently, two close C–OH condense a H_2O molecule (water droplets can be observed in the quartz tube outlet), and produce a C–O species which can be re-oxidized to C=O group by O_2 .

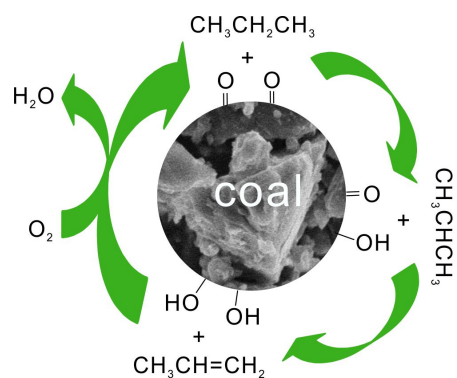


Figure 8. Scheme of proposed mechanism for catalysis of propane to propene by coal.

3. Materials and Methods

3.1. Materials

All kinds of coal powder from different suppliers were used without further treatment. The coals purchased from LANKE ENVIRON. TECH. Co., Ltd. (Dayugou coal mine, Zhengzhou city, China), HONGYAO MINERALS Co., Ltd. (Taihang mountain, Lingshou county, Shijiazhuang city, China), and YANXI MINERALS Co., Ltd. (Lingshou county, Shijiazhuang city, China) were named as L-coal, H-coal, and Y-coal, respectively. Activated carbon, black carbon, and graphite were purchased from Sinopharm Group Co., Ltd. (Shanghai, China) Boron nitride was purchased from Sigma-Aldrich Inc. (St. Louis, MO, USA) Glucose (Aladdin Co., Ltd., Beijing, China) carbonized in N_2 and NH_3 at $800\text{ }^{\circ}\text{C}$ for 2 h were labeled as carbonized glucose in N_2 and carbonized glucose in NH_3 , respectively. L-coal powder after reaction under 30 kPa P_{O_2} was named as overused L-coal powder. The

used L-coal is the raw L-coal after reaction under 7.5 kPa O₂ at temperature below 500 °C. L-coal powder after burning out at 700 °C for 2 h under air atmosphere was marked as coal residue.

3.2. Characterization

Field emission scanning electron microscopy (SEM) on a Hitachi New Generation SU8100 apparatus was used to study the microstructures of samples. X-ray photoelectron spectrum (XPS) was obtained on a Thermo Scientific Escalab 250. Electron paramagnetic resonance (EPR) spectra were collected by Bruker model A300 spectrometer. Thermo gravimetric analysis (TGA) and differential scanning calorimetry (DSC) were carried out in flowing air atmosphere (20 mL/min, heating rate: 10 °C/min) using a Netzsch STA 449F3 thermoanalyzer with alumina crucibles. Attenuated Total internal Reflectance Fourier Transform Infrared (ATR-FTIR) spectroscopy was performed on a Nicolet iS50. X-ray diffraction (XRD) data were collected using a Bruker D8 advance X-ray diffractometer. N₂ adsorption–desorption isotherm of samples was collected at 77 K on a Micromeritics 3 Flex 3500.

3.3. Catalytic Activity Test

The selective oxidative dehydrogenation (ODH) reaction was carried out at atmospheric pressure in a fixed-bed reactor. Coal powder (300 mg, powder samples except as otherwise noted) was putted into a U-type quartz tube (inner diameter 4 mm, external diameter 6 mm) between two quartz wool plugs except as otherwise noted, and then it was placed in a vertical furnace to obtain target reaction temperature. The feed gas consisting of nitrogen, oxygen, and propane can be controlled by using a Sevenstar mass flow meter with total flow rate 20 mL/min unless otherwise noted. The product components were analyzed on an on-line gas chromatography Pannatek A90 equipped with a flame ionization detector (FID). Propane conversion, product selectivity, and yield were calculated as follows:

$$\text{C}_3\text{H}_8 \text{ Conversion}(\%) = \frac{\text{C}_3\text{H}_8 \text{ In} - \text{C}_3\text{H}_8 \text{ Out}}{\text{C}_3\text{H}_8 \text{ In}} \%$$

$$\text{C}_3\text{H}_6 \text{ Selectivity}(\%) = \frac{\text{C}_3\text{H}_6 \text{ Out}}{\text{C}_3\text{H}_8 \text{ In} - \text{C}_3\text{H}_8 \text{ Out}} \%$$

$$\text{C}_3\text{H}_6 \text{ Yield}(\%) = \text{C}_3\text{H}_8 \text{ Conversion}(\%) * \text{C}_3\text{H}_6 \text{ Selectivity}(\%)$$

where C₃H₈ In and C₃H₈ Out represent the concentration of C₃H₈ at the inlet and outlet of reactor, respectively. C₃H₆ Out is the concentration of C₃H₆ at the outlet of reactor. The kinetic results were acquired from the catalytic activity testing results. The apparent activation energy (E_a) was obtained from the Arrhenius equation:

$$k = A \exp(-E_a/RT) \quad (1)$$

where *k* represents rate constant, T represents Kelvin temperature, R is the gas constant. The rate constant *k* can be replaced by N_{C₃H₈}X_{C₃H₈}/W_{cat}S_{BET} [26], where N_{C₃H₈} is C₃H₈ flow rate (mmol·s⁻¹), X_{C₃H₈} is the conversion of C₃H₈, W_{cat} is on behalf of the catalyst weight, and S_{BET} is the specific surface area of the catalyst. In this system, W_{cat} and S_{BET} are constant. Therefore, Equation (1) can be transformed into:

$$\ln(N_{\text{C}_3\text{H}_8} X_{\text{C}_3\text{H}_8}) = \ln A - E_a/RT \quad (2)$$

E_a can be obtained from the slope of the corresponding plot (ln*k* versus 1/T).

The Materials and Methods should be described with sufficient details to allow others to replicate and build on the published results. Please note that the publication of your manuscript implicates that you must make all materials, data, computer code, and protocols associated with the publication available to readers. Please disclose at the submission stage

any restrictions on the availability of materials or information. New methods and protocols should be described in detail while well-established methods can be briefly described and appropriately cited.

Research manuscripts reporting large datasets that are deposited in a publicly available database should specify where the data have been deposited and provide the relevant accession numbers. If the accession numbers have not yet been obtained at the time of submission, please state that they will be provided during review. They must be provided prior to publication.

4. Conclusions

In summary, raw coal was used as a catalyst for the oxidative dehydrogenation of propane to propene and exhibited good performance (e.g., above 90% selectivity and 8.4% yield for L-coal ($12,000 \text{ mL} \cdot (\text{h} \cdot \text{g} \cdot \text{cat})^{-1}$ mass space velocity)). The productivity is up to $2.84 \text{ gC}_3\text{H}_6 \text{ g}_{\text{cat}}^{-1} \text{ h}^{-1}$, which is better than that of many metal-based catalysts. Moreover, further thermodynamic and kinetic studies on oxidative dehydrogenation of propane were conducted, proving the first-order rate dependence with respect to propane under low oxygen or propane partial pressures. Through the EPR and XPS analysis, we found that the carbonyl groups in coal serve as active sites to activate and convert propane to propene. Although this work is a preliminary study for the use of coal as catalysts and needs to be further developed, coal as a widespread raw material holds great promise for application in catalysis.

Supplementary Materials: The following supporting information can be downloaded at: <https://www.mdpi.com/article/10.3390/catal13030628/s1>. Figure S1: Photos of various coals. Figure S2: N₂ adsorption–desorption isothermal curve of various coal powders. Figure S3: Propane conversion of active carbon, glucose carbonized in N₂ or NH₃. Figure S4: (a) The conversion of the oxidative dehydrogenation of propane for L-coal and the carbon balance when excluding and involving CO_x in the calculation. (b) Comparison between the carbon balance involving CO_x and TG result in the temperature range 350 to 550 °C. Figure S5: The catalytic activity of L-coal, overused L-coal, and coal residue. Figure S6: XRD patterns of L-coal and used L-coal. Figure S7: SEM images of (a) L-coal powder and (b) used L-coal powder. Figure S8: IR spectra of L-coal and used L-coal.

Author Contributions: Conceptualization, Q.L. and C.H.; methodology, Q.L. and M.S.; investigation, Q.L.; writing—original draft preparation, Q.L. and Y.W.; writing—review and editing, C.H. and Y.Z.; supervision, C.H.; funding acquisition, C.H. All authors have read and agreed to the published version of the manuscript.

Funding: This research was funded by National Natural Science Foundation of China (Nos. U1662112, 21273038, 21543002 and 11305091) and the Open Project Program of the State Key Laboratory of Photocatalysis on Energy and Environment (Grant Nos. SKLPEE-KF201703, SKLPEE-KF201807), Fuzhou University.

Data Availability Statement: All relevant data are within the paper.

Conflicts of Interest: The authors declare no conflict of interest.

References

1. Amghizar, I.; Avandewalle, L.; Geem, K.M.; Bmarin, G. New Trends in Olefin Production. *Engineering* **2017**, *3*, 171–178. [[CrossRef](#)]
2. Cavani, F.; Ballarini, N.; Cericola, A. Oxidative Dehydrogenation of Ethane and Propane: How Far from Commercial Implementation? *Catal. Today* **2007**, *127*, 113–131. [[CrossRef](#)]
3. Sattler, J.J.H.B.; Ruiz-Martinez, J.; Santillan-Jimenez, E.; Weckhuysen, B.M. Catalytic Dehydrogenation of Light Alkanes on Metals and Metal Oxides. *Chem. Rev.* **2014**, *114*, 10613–10653. [[CrossRef](#)] [[PubMed](#)]
4. Cherian, M.; Rao, M.S.; Yang, W.-T.; Jehng, J.-M.; Hirt, A.M.; Deo, G. Oxidative Dehydrogenation of Propane over Cr₂O₃/Al₂O₃ and Cr₂O₃ Catalysts: Effects of Loading, Precursor and Surface Area. *Appl. Catal. A* **2002**, *233*, 21–33. [[CrossRef](#)]
5. Duprez, D.; Hadj-Aissa, M.; Barbier, J. Effect of Steam on the Coking of Platinum Catalysts: I. Inhibiting Effect of Steam at Low Partial Pressure for the Dehydrogenation of Cyclopentane and the Coking Reaction. *Appl. Catal.* **1989**, *49*, 67–74. [[CrossRef](#)]
6. Zhang, X.; Gong, J.; Wei, X.; Liu, L. Increased Light Olefin Production by Sequential Dehydrogenation and Cracking Reactions. *Catalysts* **2022**, *12*, 1457. [[CrossRef](#)]

7. Carrero, C.A.; Schloegl, R.; Wachs, I.E.; Schomaecker, R. Critical Literature Review of the Kinetics for the Oxidative Dehydrogenation of Propane over Well-Defined Supported Vanadium Oxide Catalysts. *ACS Catal.* **2014**, *4*, 3357–3380. [[CrossRef](#)]
8. Chernov, A.N.; Sobolev, V.I.; Gerasimov, E.Y.; Koltunov, K.Y. Propane Dehydrogenation on Co-N-C/SiO₂ Catalyst: The Role of Single-Atom Active Sites. *Catalysts* **2022**, *12*, 1262. [[CrossRef](#)]
9. Chen, K.; Iglesia, E.; Bell, A.T. Kinetic Isotopic Effects in Oxidative Dehydrogenation of Propane on Vanadium Oxide Catalysts. *J. Catal.* **2000**, *192*, 197–203. [[CrossRef](#)]
10. Madeira, L.M.; Portela, M.F. Catalytic Oxidative Dehydrogenation of N-Butane. *Catal. Rev.* **2002**, *44*, 247–286. [[CrossRef](#)]
11. Bulánek, R.; Čičmanec, P.; Sheng-Yang, H.; Knotek, P.; Čapek, L.; Setnička, M. Effect of Preparation Method on Nature and Distribution of Vanadium Species in Vanadium-Based Hexagonal Mesoporous Silica Catalysts: Impact on Catalytic Behavior in Propane Odh. *Appl. Catal. A* **2012**, *415*, 29–39. [[CrossRef](#)]
12. Santacesaria, E.; Cozzolino, M.; Di Serio, M.; Venezia, A.; Tesser, R. Vanadium Based Catalysts Prepared by Grafting: Preparation, Properties and Performances in the Odh of Butane. *Appl. Catal. A* **2004**, *270*, 177–192. [[CrossRef](#)]
13. Tsilomelekis, G.; Christodoulakis, A.; Boghosian, S. Support Effects on Structure and Activity of Molybdenum Oxide Catalysts for the Oxidative Dehydrogenation of Ethane. *Catal. Today* **2007**, *127*, 139–147. [[CrossRef](#)]
14. Chen, K.; Xie, S.; Bell, A.T.; Iglesia, E. Alkali Effects on Molybdenum Oxide Catalysts for the Oxidative Dehydrogenation of Propane. *J. Catal.* **2000**, *195*, 244–252. [[CrossRef](#)]
15. Chaar, M.A.; Patel, D.; Kung, H.H. Selective Oxidative Dehydrogenation of Propane over V-Mg-O Catalysts. *J. Catal.* **1988**, *109*, 463–467. [[CrossRef](#)]
16. Abello, M.C.; Gomez, M.F.; Ferretti, O. Mo/Γ-Al₂O₃ Catalysts for the Oxidative Dehydrogenation of Propane.: Effect of Mo Loading. *Appl. Catal. A* **2001**, *207*, 421–431. [[CrossRef](#)]
17. Duruibe, J.O.; Ogwuegbu, M.; Ekwurugwu, J. Heavy Metal Pollution and Human Biotoxic Effects. *Int. J. Phys. Sci.* **2007**, *2*, 112–118.
18. Mamedov, E.; Corberán, V.C. Oxidative Dehydrogenation of Lower Alkanes on Vanadium Oxide-Based Catalysts. The Present State of the Art and Outlooks. *Appl. Catal. A* **1995**, *127*, 1–40. [[CrossRef](#)]
19. Mestl, G.; Maksimova, N.I.; Keller, N.; Roddatis, V.V.; Schlögl, R. Carbon Nanofilaments in Heterogeneous Catalysis: An Industrial Application for New Carbon Materials? *Angew. Chem. Int. Ed.* **2001**, *40*, 2066–2068.
20. Keller, N.; Maksimova, N.I.; Roddatis, V.V.; Schur, M.; Mestl, G.; Butenko, Y.V.; Kuznetsov, V.L.; Schlögl, R. The Catalytic Use of Onion-Like Carbon Materials for Styrene Synthesis by Oxidative Dehydrogenation of Ethylbenzene. *Angew. Chem. Int. Ed.* **2002**, *41*, 1885–1888. [[CrossRef](#)]
21. Zhang, J.; Liu, X.; Blume, R.; Zhang, A.; Schlögl, R.; Su, D.S. Surface-Modified Carbon Nanotubes Catalyze Oxidative Dehydrogenation of N-Butane. *Science* **2008**, *322*, 73–77. [[CrossRef](#)] [[PubMed](#)]
22. Zhang, J.; Su, D.S.; Blume, R.; Schlögl, R.; Wang, R.; Yang, X.; Gajović, D.A. Surface Chemistry and Catalytic Reactivity of a Nanodiamond in the Steam-Free Dehydrogenation of Ethylbenzene. *Angew. Chem. Int. Ed.* **2010**, *49*, 8640–8644. [[CrossRef](#)] [[PubMed](#)]
23. Liang, C.; Xie, H.; Schwartz, V.; Howe, J.; Dai, S.; Overbury, S.H. Open-Cage Fullerene-Like Graphitic Carbons as Catalysts for Oxidative Dehydrogenation of Isobutane. *J. Am. Chem. Soc.* **2009**, *131*, 7735–7741. [[CrossRef](#)] [[PubMed](#)]
24. Su, D.S.; Delgado, J.J.; Liu, X.; Wang, D.; Schlögl, R.; Wang, L.; Zhang, Z.; Shan, Z.; Xiao, F.S. Highly Ordered Mesoporous Carbon as Catalyst for Oxidative Dehydrogenation of Ethylbenzene to Styrene. *Chem.-Asian J.* **2009**, *4*, 1108–1113. [[CrossRef](#)] [[PubMed](#)]
25. Velásquez, J.d.J.D.; Suárez, L.M.C.; Figueiredo, J.L. Oxidative Dehydrogenation of Isobutane over Activated Carbon Catalysts. *Appl. Catal. A* **2006**, *311*, 51–57. [[CrossRef](#)]
26. Hu, Z.-P.; Zhao, H.; Chen, C.; Yuan, Z.-Y. Castanea Mollissima Shell-Derived Porous Carbons as Metal-Free Catalysts for Highly Efficient Dehydrogenation of Propane to Propylene. *Catal. Today* **2018**, *316*, 214–222. [[CrossRef](#)]
27. Grant, J.T.; Carrero, C.A.; Goeltl, F.; Venegas, J.; Mueller, P.; Burt, S.P.; Specht, S.E.; McDermott, W.P.; Chieregato, A.; Hermans, I. Selective Oxidative Dehydrogenation of Propane to Propene Using Boron Nitride Catalysts. *Science* **2016**, *354*, 1570–1573. [[CrossRef](#)]
28. Shafiee, S.; Topal, E. When Will Fossil Fuel Reserves Be Diminished? *Energy Policy* **2009**, *37*, 181–189. [[CrossRef](#)]
29. Zhang, G.; Dong, Y.; Feng, M.; Zhang, Y.; Zhao, W.; Cao, H. CO₂ Reforming of CH₄ in Coke Oven Gas to Syngas over Coal Char Catalyst. *Chem. Eng. J.* **2010**, *156*, 519–523. [[CrossRef](#)]
30. Maldonado-Hódar, F.J.; Madeira, L.M.; Portela, M.F. The Use of Coals as Catalysts for the Oxidative Dehydrogenation of N-Butane. *Appl. Catal. A* **1999**, *178*, 49–60. [[CrossRef](#)]
31. Sun, X.; Ding, Y.; Zhang, B.; Huang, R.; Chen, D.; Su, D.S. Insight into the Enhanced Selectivity of Phosphate-Modified Annealed Nanodiamond for Oxidative Dehydrogenation Reactions. *ACS Catal.* **2015**, *5*, 2436–2444. [[CrossRef](#)]
32. Hu, Z.-P.; Chen, C.; Ren, J.-T.; Yuan, Z.-Y. Direct Dehydrogenation of Propane to Propylene on Surface-Oxidized Multiwall Carbon Nanotubes. *Appl. Catal. A* **2018**, *559*, 85–93. [[CrossRef](#)]
33. Grabowski, R.; Grzybowska, B.; Samson, K.; Słoczyński, J.; Stoch, J.; Wcisło, K. Effect of Alkaline Promoters on Catalytic Activity of V₂O₅/TiO₂ and MoO₃/TiO₂ Catalysts in Oxidative Dehydrogenation of Propane and in Isopropanol Decomposition. *Appl. Catal. A* **1995**, *125*, 129–144. [[CrossRef](#)]
34. Grant, J.T.; Venegas, J.M.; McDermott, W.P.; Hermans, I. Aerobic Oxidations of Light Alkanes over Solid Metal Oxide Catalysts. *Chem. Rev.* **2018**, *118*, 2769–2815. [[CrossRef](#)]

35. Glushkov, D.O.; Strizhak, P.A.; Vysokomornaya, O.V. Numerical Research of Heat and Mass Transfer During Low-Temperature Ignition of a Coal Particle. *Therm. Sci.* **2015**, *19*, 285–294. [[CrossRef](#)]
36. Chen, K.; Khodakov, A.; Yang, J.; Bell, A.T.; Iglesia, E. Isotopic Tracer and Kinetic Studies of Oxidative Dehydrogenation Pathways on Vanadium Oxide Catalysts. *J. Phys. Chem. B* **2001**, *105*, 325–333. [[CrossRef](#)]
37. Qi, W.; Yan, P.; Su, D.S. Oxidative Dehydrogenation on Nanocarbon: Insights into the Reaction Mechanism and Kinetics Via in Situ Experimental Methods. *Acc. Chem. Res.* **2018**, *51*, 640–648. [[CrossRef](#)]
38. Zhou, L.; Chen, J.; Ji, C.; Zhou, L.; O'Brien, P. A Facile Solid Phase Reaction to Prepare TiO₂ Mesocrystals with Exposed {001} Facets and High Photocatalytic Activity. *CrystEngComm* **2013**, *15*, 5012–5015. [[CrossRef](#)]
39. Chen, K.; Bell, A.T.; Iglesia, E. Kinetics and Mechanism of Oxidative Dehydrogenation of Propane on Vanadium, Molybdenum, and Tungsten Oxides. *J. Phys. Chem. B* **2000**, *104*, 1292–1299. [[CrossRef](#)]
40. Petrakis, L.; Grandy, D.W. Electron Spin Resonance Spectrometric Study of Free Radicals in Coals. *Anal. Chem.* **1978**, *50*, 303–308. [[CrossRef](#)]
41. Liu, J.; Jiang, X.; Shen, J.; Zhang, H. Influences of Particle Size, Ultraviolet Irradiation and Pyrolysis Temperature on Stable Free Radicals in Coal. *Powder Technol.* **2015**, *272*, 64–74. [[CrossRef](#)]
42. Yangdong, O.; Liwen, G. Research on the Influence of Oxygen-Containing Functional Group and Gas Emission by Coal Seams. *Energy Procedia* **2012**, *17*, 1901–1906. [[CrossRef](#)]
43. Liu, J.; Jiang, X.; Shen, J.; Zhang, H. Chemical Properties of Superfine Pulverized Coal Particles. Part 1. Electron Paramagnetic Resonance Analysis of Free Radical Characteristics. *Adv. Powder Technol.* **2014**, *25*, 916–925. [[CrossRef](#)]
44. Qi, W.; Liu, W.; Zhang, B.; Gu, X.; Guo, X.; Su, D. Oxidative Dehydrogenation on Nanocarbon: Identification and Quantification of Active Sites by Chemical Titration. *Angew. Chem. Int. Ed.* **2013**, *52*, 14224–14228. [[CrossRef](#)]
45. Rozanska, X.; Fortrie, R.; Sauer, J. Oxidative Dehydrogenation of Propane by Monomeric Vanadium Oxide Sites on Silica Support. *J. Phys. Chem. C* **2007**, *111*, 6041–6050. [[CrossRef](#)]
46. Mao, S.; Li, B.; Su, D. The First Principles Studies on the Reaction Pathway of the Oxidative Dehydrogenation of Ethane on the Undoped and Doped Carbon Catalyst. *J. Mater. Chem. A* **2014**, *2*, 5287–5294. [[CrossRef](#)]
47. Govindasamy, A.; Muthukumar, K.; Yu, J.; Xu, Y.; Gulians, V.V. Adsorption of Propane, Isopropyl, and Hydrogen on Cluster Models of the M1 Phase of Mo–V–Te–Nb–O Mixed Metal Oxide Catalyst. *J. Phys. Chem. C* **2010**, *114*, 4544–4549. [[CrossRef](#)]
48. Guo, X.L.; Qi, W.; Liu, W.; Yan, P.Q.; Li, F.; Liang, C.H.; Su, D.S. Oxidative Dehydrogenation on Nanocarbon: Revealing the Catalytic Mechanism Using Model Catalysts. *ACS Catal.* **2017**, *7*, 1424–1427. [[CrossRef](#)]
49. Liu, L.; Deng, Q.-F.; Agula, B.; Zhao, X.; Ren, T.-Z.; Yuan, Z.-Y. Ordered Mesoporous Carbon Catalyst for Dehydrogenation of Propane to Propylene. *Chem. Commun.* **2011**, *47*, 8334–8336. [[CrossRef](#)]
50. Liu, L.; Deng, Q.-F.; Agula, B.; Ren, T.-Z.; Liu, Y.-P.; Zhaorigetu, B.; Yuan, Z.-Y. Synthesis of Ordered Mesoporous Carbon Materials and Their Catalytic Performance in Dehydrogenation of Propane to Propylene. *Catal. Today* **2012**, *186*, 35–41. [[CrossRef](#)]

Disclaimer/Publisher's Note: The statements, opinions and data contained in all publications are solely those of the individual author(s) and contributor(s) and not of MDPI and/or the editor(s). MDPI and/or the editor(s) disclaim responsibility for any injury to people or property resulting from any ideas, methods, instructions or products referred to in the content.